Bulletin of the Mineral Research and Exploration

http://bulletin.mta.gov.tr

Assessment of crustal thinning and tectonic stress distribution of Gülbahçe fault zone and its surroundings (İzmir, West Türkiye) using gravity and magnetic anomalies

Oya ANKAYA PAMUKÇU[a*] , Ayça ÇIRMIK[a] , Fikret DOĞRU[b] , Ece ÜNLÜ[a] and Barış Can MALALİÇİ[c]

[a]Dokuz Eylül University, Engineering Faculty, Department of Geophysical Engineering, İzmir, Türkiye
[b]Atatürk University, Oltu Vocational College, Construction, Erzurum, Türkiye
[c]General Directorate of Mineral Research and Exploration, Ankara, Türkiye

Research Article

ABSTRACT

Gülbahçe Fault Zone (GFZ) is a significant tectonic structure and seismic source for İzmir city and its surroundings. The major earthquakes occurred at the surroundings of GFZ are 2005 Seferihisar, 2020 Samos Island-Aegean Sea and 2021 Seferihisar earthquakes. In this study, the crustal thinning and tectonic stress distribution of GFZ and its surroundings were analyzed by using the new gravity and magnetic data. The correspondence analysis was applied by appraising together the magnetic and free-air anomaly data. Moreover, the average density of the subsurface structure was calculated by applying the Parasnis method. The deviatoric stress calculation was executed and the change of the physical properties that controls the gravity and magnetic anomaly of the crustal structure of the GFZ and its surroundings from north to south was investigated. Therefore, the average density values, which were obtained from gravity anomalies, were computed as 2.59 gr / cm^3 in the north of the study region and it decreased to 2.06, 1.8 and 1.49 gr / cm^3 towards to the south. The free-air gravity anomaly values were between 0-70 mGal and the magnetic anomalies were between -450-150 nT. The deviatoric stress values were between -0.2-0.1 MPa.

1. Introduction

The study area is the N - S trending GFZ and its surroundings which separate Karaburun Peninsula from İzmir Gulf (Emre et al., 2005) (Figure 1). Western Anatolia including study area which is located in the Alpine - Himalayan orogenic belt, is the part of the wide - ranging compression zone between the Arabian, African and Eurasian plates (Pamukçu and Yurdakul, 2008; Çırmık et al., 2016; Çırmık et al., 2017*a, b*; Çırmık and Pamukçu, 2017; Doğru et al., 2017, 2018; Doğru and Pamukçu, 2019; Pamukçu et al., 2019). Western Anatolia is tectonically active and

is one of the rapidly deforming and extending areas in the world (Dewey and Şengör, 1979; Ambraseys, 1988; Taymaz et al., 1991; Bozkurt, 2001; Pamukçu and Yurdakul, 2008; Pamukçu et al., 2012, 2013). Western Anatolia has N - S trending extension from the Miocene to present (Dewey and Şengör, 1979; Şengör et al., 1985). As a result of the collision of Arabian and Eurasian plates in southeastern Anatolia, the North Anatolian and East Anatolian Fault zones occurred and the Anatolian plate has moved counter - clockwise towards the west (Şengör and Yılmaz, 1981). The westward movement of the Anatolian plate (Aktuğ and Kılıçoğlu, 2006) and the northward plunge

of the African plate under the southern Anatolia plate along the Aegean - Cyprus subduction zone have formed the N - S trending extensional tectonics of the western Anatolia (Şengör and Yılmaz, 1981) and have caused the Anatolian block to escape to the east (Ketin, 1948; McKenzie, 1972; Barka and Kadinsky - Cade, 1988).

Emre et al. (2005) pointed out that the dominant sense of the GFZ is strike - slipe. The submarine data of Ocakoğlu et al. (2005) represented that the GFZ includes inverse fault component along the north segment and the western block of the fault is pushed on to the eastern block (Emre et al., 2005).

The previous studies (Akıncı et al., 2000; Çetiner, 2012; Pamukçu et al., 2013, 2015; Çırmık et al., 2016; Çırmık et al., 2017*a, b*; Malaliçi, 2019) showed that İzmir and its surroundings represent a high risk in terms of earthquakes. Particularly, the 17 October - 21 October 2005 Sığacık Bay earthquake series ($M_l = 5.7$, $M_l = 5.9$), 12 June 2017 Karaburun - Lesvos Island offshore earthquake ($M_w = 6.3$) and 30 October 2020 Samos Island earthquake ($M_w = 6.9$) were the most effective earthquakes for the study region. In addition, the tsunami was observed in the south of the study region immediately after 2020 Samos Island earthquake (Sözbilir et al., 2020). This seismically active region has studied since 2009 by Pamukçu et al. (2013, 2015); Çırmık et al. (2016); Çırmık et al. (2017*a, b*) and Malaliçi (2019). In this study, the crustal thinning and tectonic stress distributions of GFZ and its surroundings were determined by using the gravity and magnetic data which were obtained up to 2019. Within the scope of this study, the crustal structure of the risky region was examined from the gravity and magnetic data obtained from the project of Dokuz Eylül University (Project No: 2018.KB.FEN.010).

These regions, which represent magnetic and gravity anomalies caused by the complex structure of the GFZ and its surroundings, reflect the physical characteristics of the crust (Pamukçu et al., 2007, 2015). Therefore, the physical characteristics of the crust of GFZ and its surrounding were determined by using correspondence analysis of gravity and magnetic data as the first study for this study region. The mean density calculations of the subsurface structure were performed with Parasnis method by using Bouguer anomaly and topography data. Finally, the deviatoric stress values (Turcotte and Schubert, 2002; Xu et al., 2015) were obtained by using the mean density and Bouguer gravity anomaly values. As a result, the findings related with the crustal structure and the previous studies were examined together.

2. Data Analysis

Gravity and magnetic data were obtained by the project founded by Dokuz Eylül University Research Foundation (Project No: DEU - BAP 2018. KB.FEN.010) and then, gravity and magnetic data were evaluated with TÜBITAK (The Scientific and Technological Research Council of Turkey, Project No: 108Y285) project. Dokuz Eylül University Tinaztepe Campus was chosen as the base point for the gravity and magnetic measurements and the base measurements were obtained twice a day (morning and evening).

The complex gravity and magnetic anomaly fields of the GFZ and its surroundings (Figure 1) provide a record of the complex features and tectonic evolution of the underlying crust. The common approach for minimizing the interpretative uncertainties is to evaluate the correlation analyses at anomalies. There are no detailed previous gravity and magnetic studies in the study area and its surroundings. Therefore, within the scope of this study, it was aimed to better examine the crustal features of the area by analysing the crust with the correlation between gravity and magnetic anomalies.

2.1. The Correlation Between Free-Air and Magnetic Anomalies

The base, latitude and free-air corrections were applied to the measured microgravity data in order to obtain free-air gravity data (Figure 2). In the next step, Reduction to the Pole (RTP) was applied to the magnetic anomaly (Figure 3).

There are many studies (e.g. Von Frese et al., 1982, 1997*a, b*; Saleh et al., 2006; Pamukçu et al., 2007; De Ritis et al., 2010; Hinze et al., 2013; Erbek and Dolmaz, 2014; Pamuk, 2019) noticing that it is important to evaluate the alignment between gravity and magnetic anomalies in the interpretation of crustal
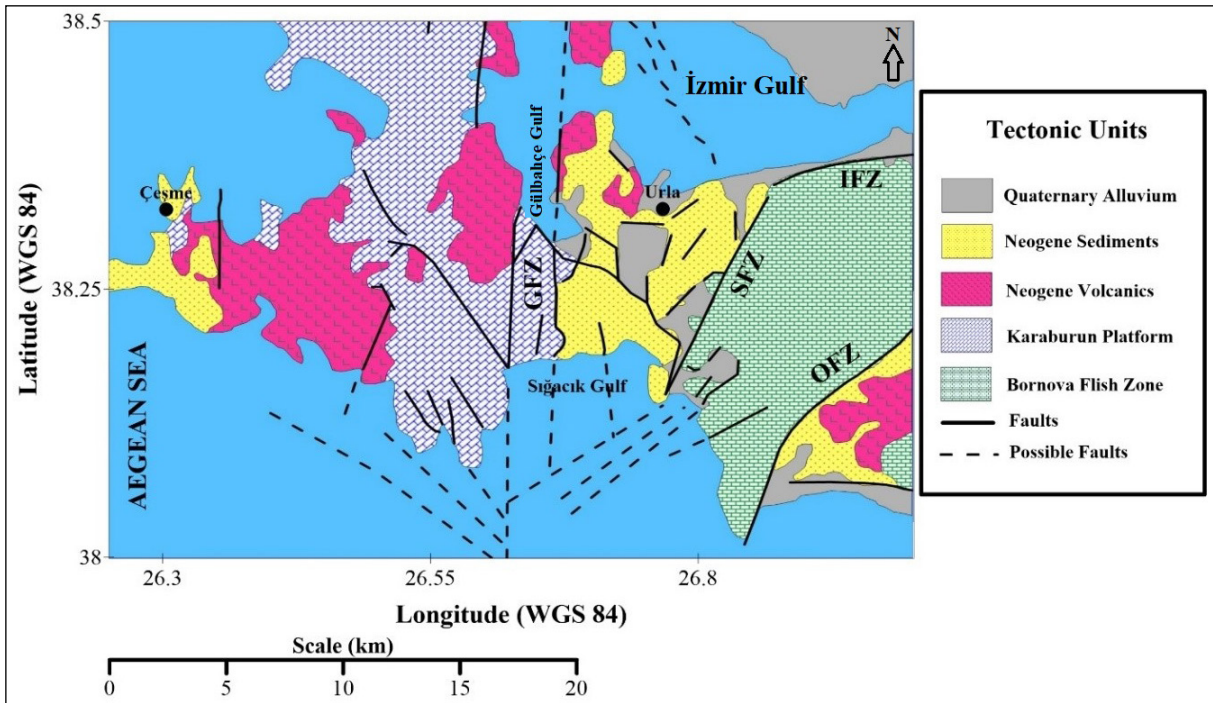
Figure 1- Simplified geological map of the study area (modified from Uzel and Sözbilir, 2008; Sözbilir et al., 2009; Uzel et al., 2012; Göktaş, 2016; Malaliçi, 2019) (GFZ: Gülbahçe Fault Zone, SFZ: Seferihisar Fault Zone, IFZ: İzmir Fault Zone, OFZ: Orhanlı Fault Zone).

properties and they pointed out that the change in crustal thicknesses can be determined by performing the correspondence analysis between gravity and magnetic anomalies.

The most important factor for gravity and magnetic data is temperature, since temperature directly affects gravity and magnetic anomalies (Von Frese et al., 1982; Pamukçu et al., 2007). In addition to these, both
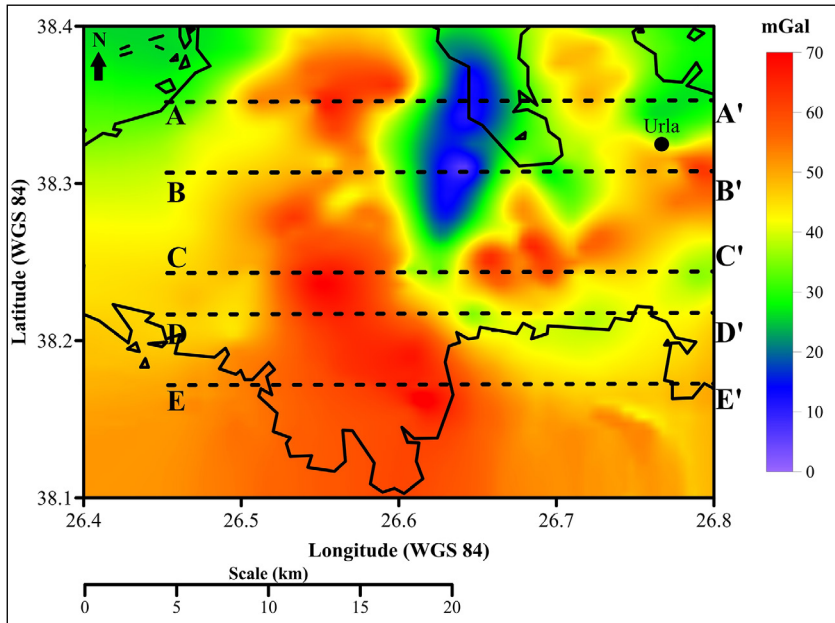
Figure 2- Free-air anomaly map of the study area.
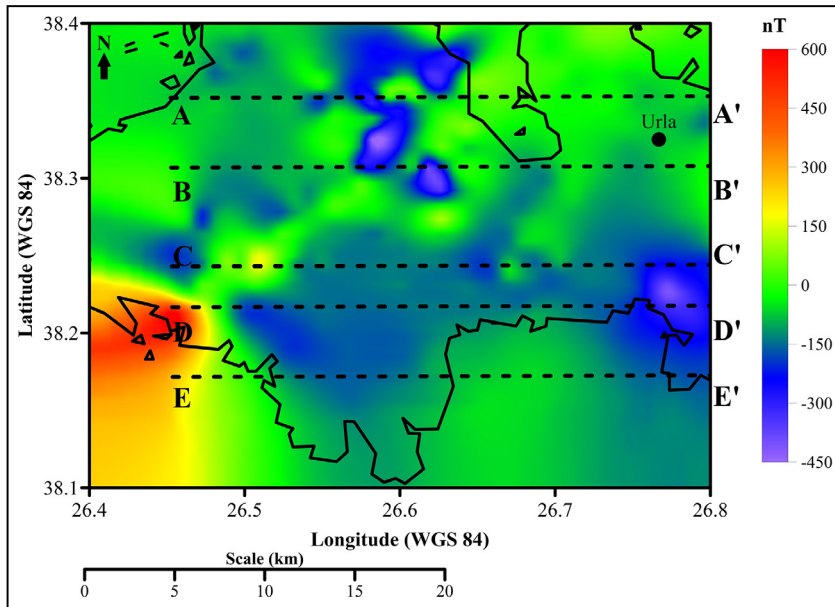
Figure 3- Reduction to the Pole (RTP) magnetic anomaly map of the study area.

surface and subsurface loads are effective on gravity. The most important parameter affecting the magnetic anomaly is the Curie temperature and depth which becomes shallower as the crust gets thinner. Thus, the amplitude of the magnetic anomaly also decreases. If this decreasing magnetic anomaly is inversely proportional to the free-air gravity anomaly including the topographic load (mass effect), then it is possible to mention the thin crust effect in that part of the study area (Von Frese et al., 1982; Pamukçu et al., 2007).

In order to perform correspondence analysis between gravity and magnetic data, five profiles were selected from free-air gravity (Figure 2) and magnetic anomaly (Figure 3) maps and the correspondence analysis of two data set were given at Figure 4.

2.2. The Correlation Between Complete Bouguer Gravity and Topography Anomalies

The relationship between Bouguer and topography values plays an important role in the analysis of crustal structure within the scope of isostasy (Watts, 2001; Pamukçu and Yurdakul, 2008; Arslan et al., 2010; Pamukçu and Akçığ, 2011; Doğru et al., 2018). According to the isostasy theorem, where the Bouguer anomaly increases, the topography anomaly is expected to decrease.

First order trend application was performed to the Bouguer anomalies (Figure 5). In 5 profiles seen in Figure 6, cross sections were taken from Bouguer and topography values (Figure 6) and the changes of two data set are given in Figure 7.

2.3. Density Determination with Parasnis Method and Calculation of Tectonic Stress

Parasnis (1952) method uses the relationship between gravity and topography variations for density determinations. The density with Parasnis method is determined as

$$\rho = \frac{0.3086 - \frac{\Delta g}{\Delta h}}{0.04191} \tag{1}$$

Here ρ is density, Δg and Δh are mean gravity and topography values, respectively. The mean crustal density values of the study area were calculated (Table 1) by using Equation 1 from the topography and free-air gravity data of the profiles shown in Figure 2. The density determination was performed for D - D′ profile in two steps and two density values were obtained (Table 1) due to the gravity anomaly changes in this profile (Figure 2).
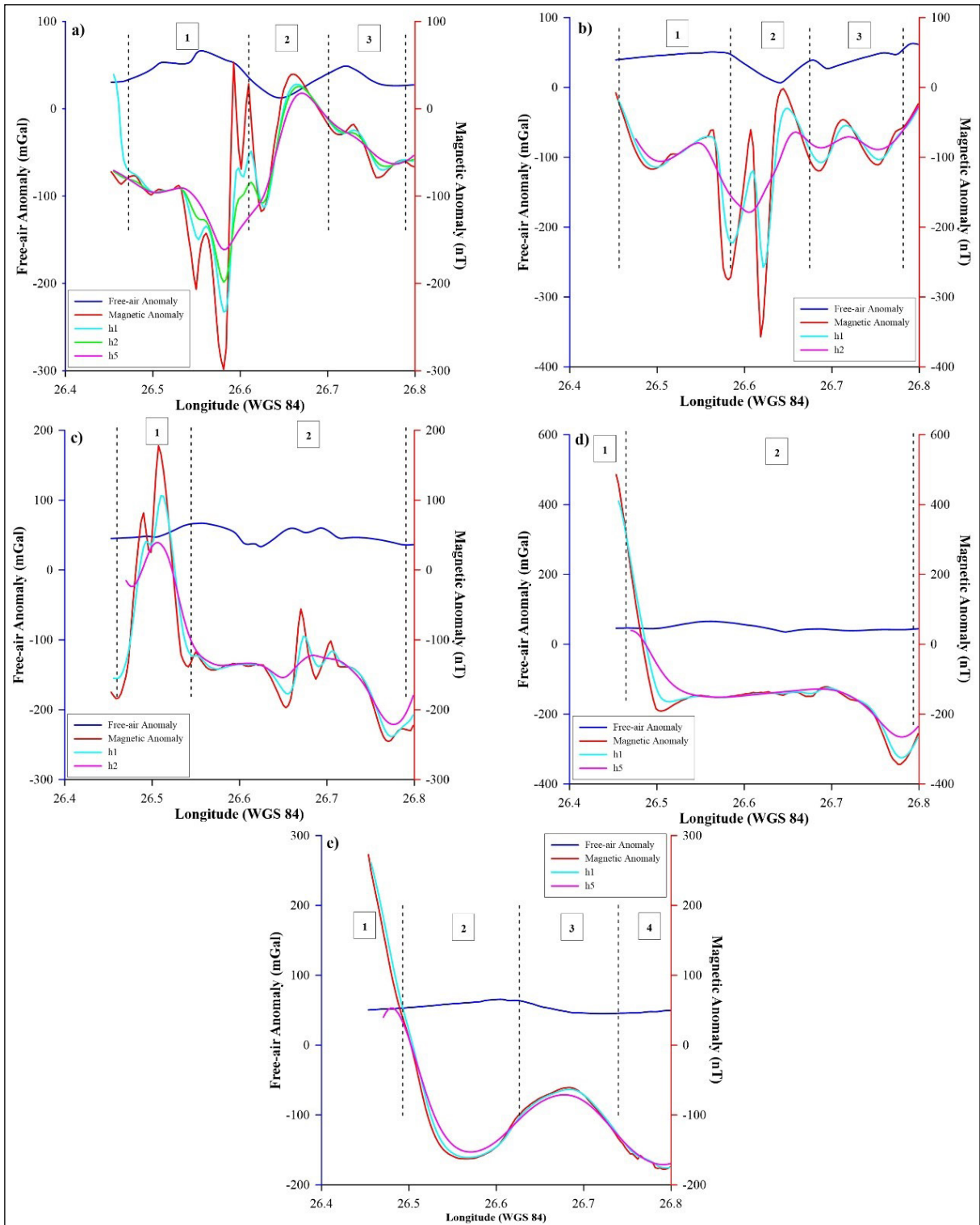
Figure 4- The correspondence analysis of the profiles taken from free-air gravity and magnetic anomaly maps; a) A - A' profile, b) B - B' profile, c) C - C' profile, d) D - D' profile, and e) E - E' profile. Blue and red lines represent free-air gravity and Reduction to the Pole (RTP) magnetic anomalies, respectively. Turquoise lines represent the upward continuation of h = 1 km, green lines represent the upward continuation of h = 2 km in Figure 4a, pink lines represent the upward continuation of h = 2 km in 4b, 4c and h = 5 km in Figure 4a, 4d, 4e.
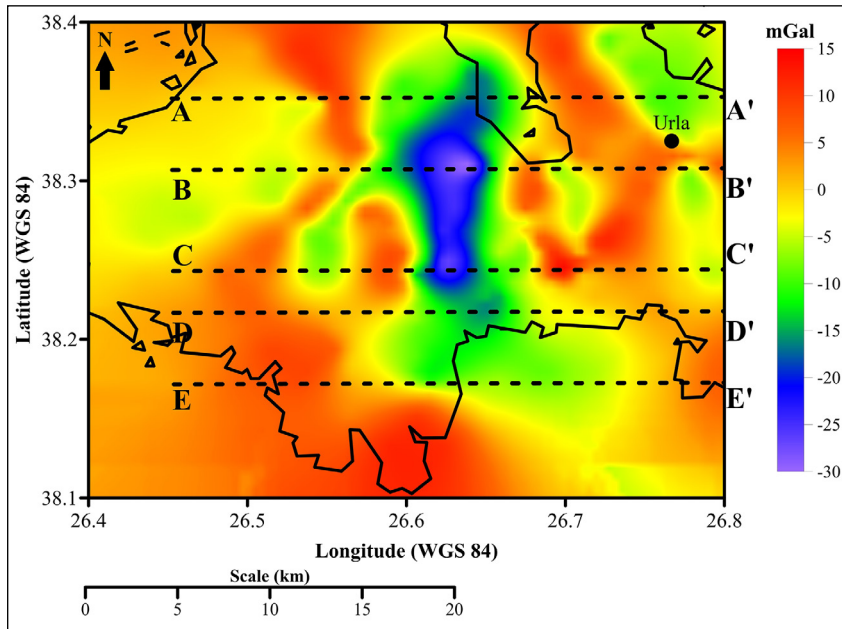
Figure 5- 1st order trend applied Bouguer gravity anomaly map and the profiles.
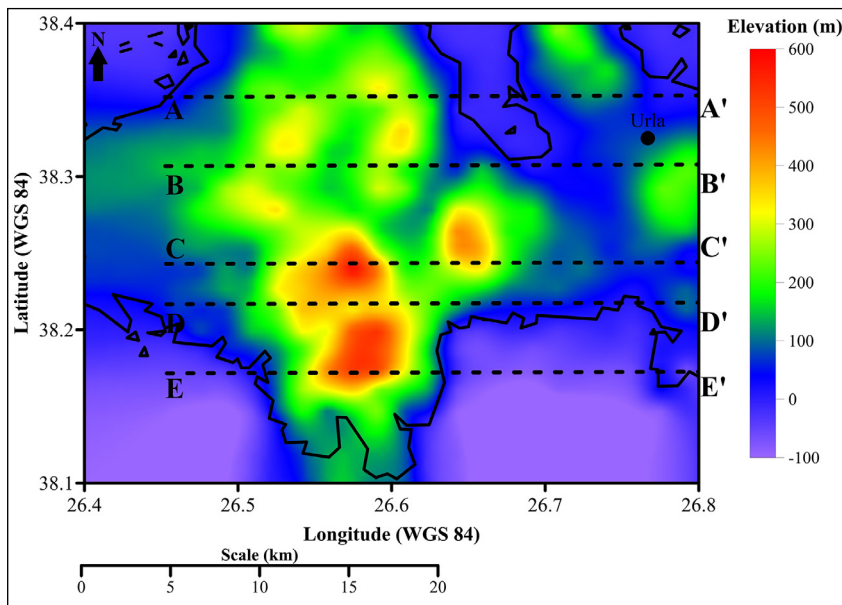
Figure 6- The topographic map and the profiles.

Table 1- The mean density values of the profiles.

Profil Name	The Mean Density values (gr / cm³)	
A - A′	2.59	
B - B′	2.06	
C - C′	2.012	
D - D′	1.40	1.80
E - E′	1.49	

The expression of lithostatic stress is given by three normal stresses and these stresses are proportional to depth. However, the lithostatic state of stress due to the isostatic equilibrium is not the same everywhere in the earth. Indeed, the horizontal normal stress consists of two components: lithostatic stress and deviatoric stress. Deviatoric stress ($\Delta\sigma_{xx}$) can be based on static equilibrium on the continent (Turcotte and Schubert, 2002) and it is given by
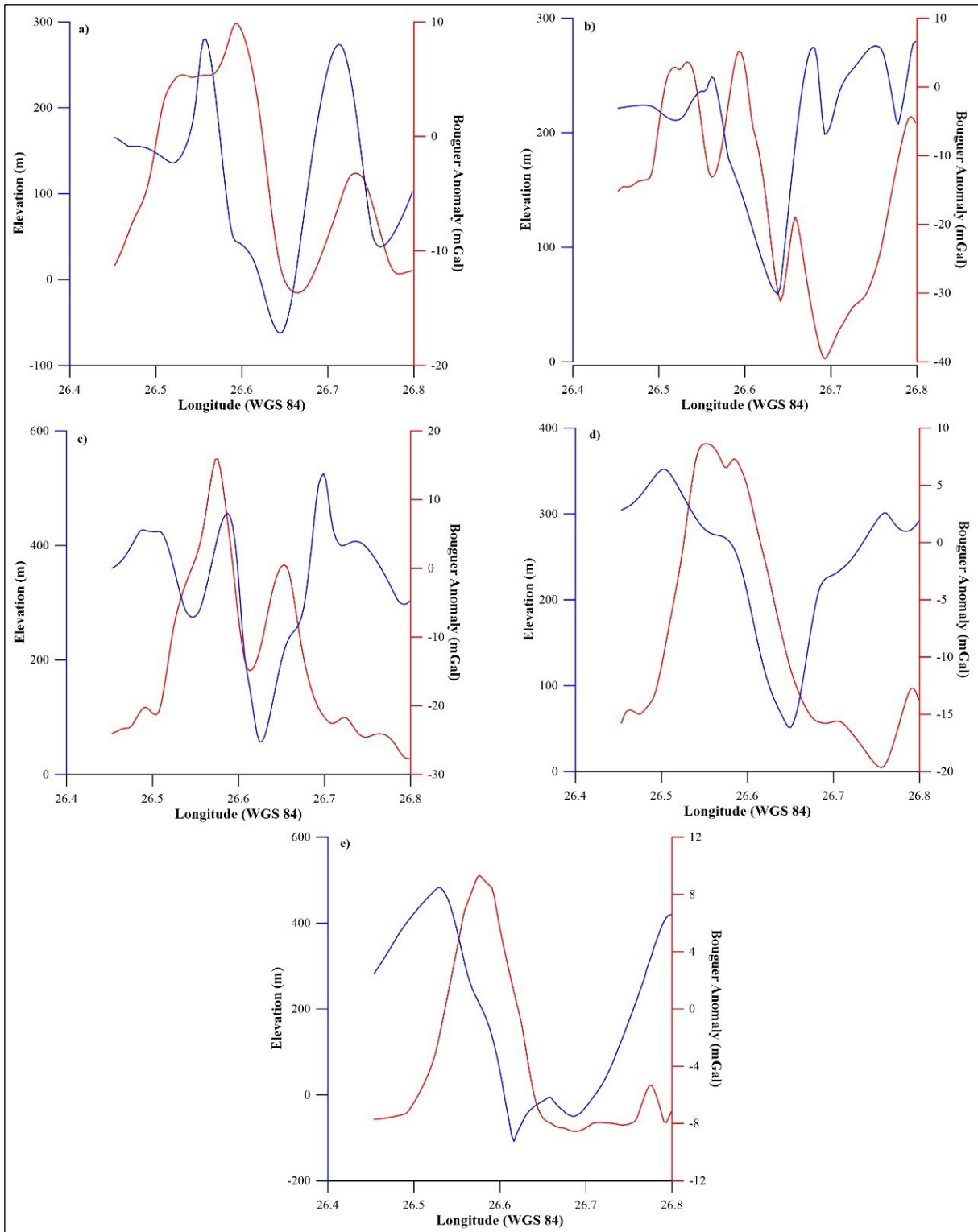
Figure 7- The profile values of the 1st order trend applied Bouguer gravity anomaly and topography maps; a) A - A' profile, b) B - B' profile, c) C - C' profile, d) D - D' profile and e) E - E' profile.

$$\Delta\sigma_{xx}=-\frac{1}{2}gh\Delta\rho\frac{\rho_c}{\rho_m} \qquad (2)$$

Here, g is gravity acceleration, h is continental thickness, ρ_c and ρ_m are the density of crust and mantle, respectively. If the Bouguer plate is considered, the vertical gravity anomaly is given by (Heiskanen and Moritz, 1967);

$$\Delta g_z=-2\pi hG\Delta\rho \qquad (3)$$

by using the local density value of each unit block $\rho_{(x,y)}$ instead of the mean density of the crust ρ_c, Equation 2 and 3 are combined and

$$\sigma_{xx}=\frac{g\rho_{(x,y)}}{4\pi G\rho_m}\Delta g_z \qquad (4)$$

is obtained. Equation 4 gives the way to find horizontal tectonic stress from the gravity anomaly (Xu et al., 2015; Pamukçu, 2017).

The deviatoric stress causes shape changes and shear stresses ascending also it controls the degree of body distortion (Aadnoy and Looyeh, 2019). Mount and Suppe (1987) pointed out that the deviatoric stress in the crust is an important unknown quantity in tectonophysics and structural geology. In the light of this knowledge, the deviatoric stress values were obtained (Figure 8) by using the mean density values calculated with Equation 4.

Additionally, the Coulomb, normal and shear stress change values of the region were calculated by using the stress values based on modelling of GNSS data and fault parameters of Çırmık et al. (2017a). These stress changes were drawn together with deviatoric stress (Figures 9, 10 and 11, respectively) for comparing the stress changes of the region.

3. Results

In the scope of this study, new microgravity and magnetic data were measured at GFZ and its surroundings (Figure 1) for investigating the crustal structure and tectonic stress distribution. Free-air gravity anomaly values of the region (Figure 2) change between 0 - 70 mGal. In Figure 2, the lowest values (from 0 mGal to ~25 mGal) are seen in the northern side and centre of GFZ (Figure 1) and the average values (~30 - 35 mGal) are seen at northern coasts of the study area. Besides, the lower values (0 - 35 mGal) are noticed at the southern coast of the Gulf of Gülbahçe (Figure 1). On the other hand, the southern coasts of the study region and the region between the longitudes 26.5° - 26.6° represent higher gravity values. Additionally, the free-air gravity values of the southern part of GFZ are higher than its northern part.

According to the RTP magnetic anomaly map (Figure 3) the values change from -450 nT to 600 nT
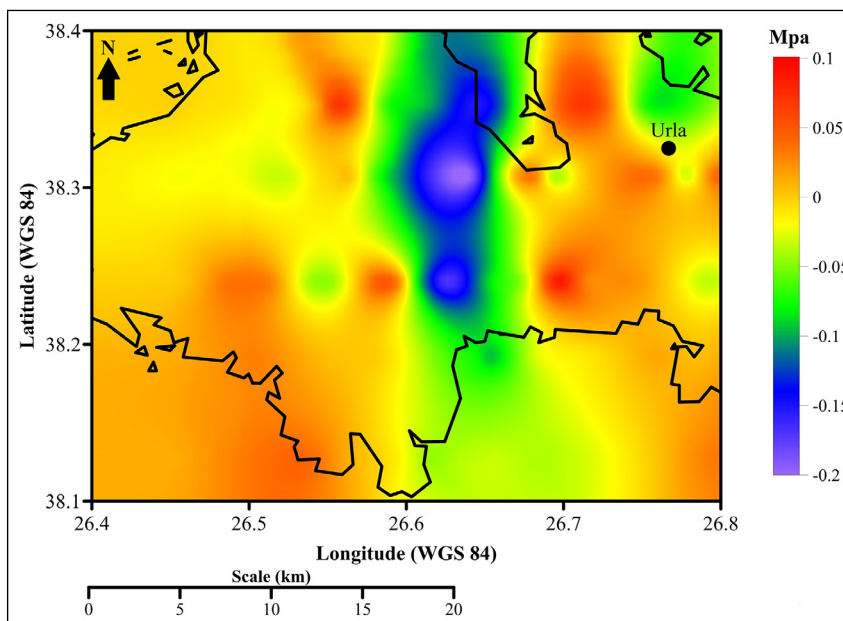
Figure 8- The deviatoric stress values obtained by gravity data and density values.
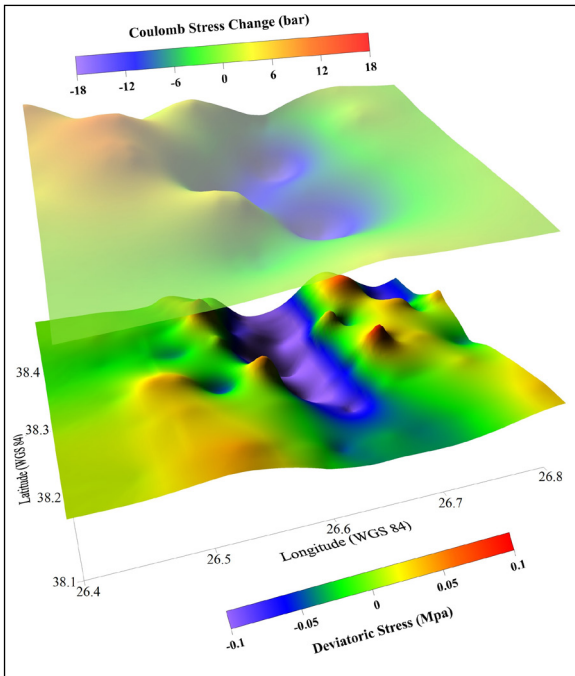
Figure 9- Coulomb stress and deviatoric stress distributions of the study area.
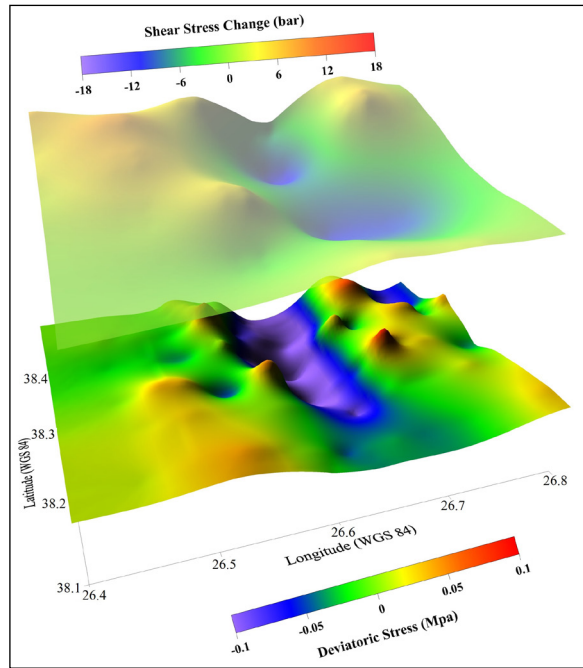
Figure 11- Shear stress and deviatoric stress distributions of the study area.
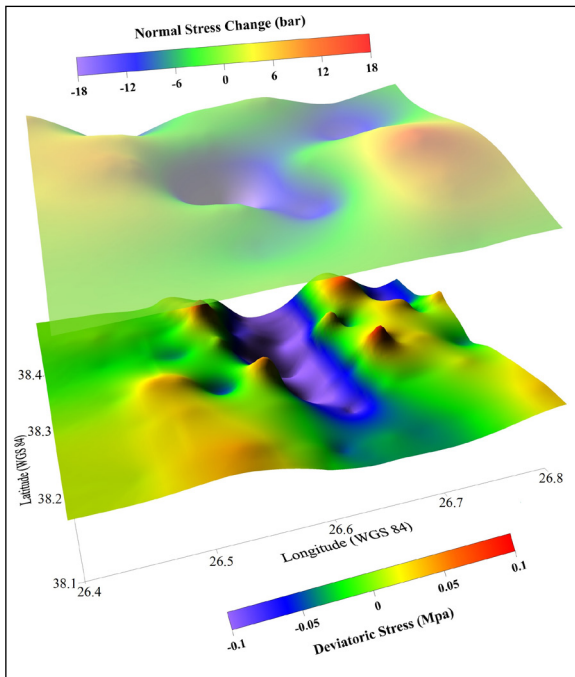
Figure 10- Normal stress and deviatoric stress distributions of the study area.

(Figure 3) but in general, the magnetic values are between 150 nT and -450 nT in the study region. While GFZ represents different (lower) gravity anomalies respect to other part of the region (Figure 2),

any anomaly difference is not seen clearly at magnetic anomaly map for GFZ (Figure 3). High positive magnetic values are remarkable between the longitudes 26.4° - ~26.47° and latitudes 38.1°- 38.2° (Figure 3).

In the next step, the cross sections were taken at 5 profiles for investigating the crustal structure of GFZ and its surroundings from the RTP magnetic, upward continuation applied magnetics and free-air gravity anomalies by using the approaches of Von Frese et al. (1982) and Pamukçu et al. (2007) (Figure 4). The correspondence analysis was performed between these data. When the correlation of free-air gravity and magnetic data are examined (Figure 4), it can be said that there is a crustal thinning where the free-air gravity and magnetic data represent inverse proportions (opposite correlation) (Von Frese et al., 1982). If the regions which represent high gravity and high magnetisations are evaluated with the geological units of the region, it is seen that these regions include the volcanic (Neogene volcanic) units (Figure 1). Therefore, it can be said that the regions which represent positive correlation (direct proportion) between gravity and magnetic anomalies (Figure 4) are related with volcanic root systems in addition to topographic components.

For analysing the profiles in detail, the profiles are divided into the regions due to the changes on gravity and magnetic values (Figure 4). In Figure 4a, which contains profile values of A - A', the profile is divided into 3 regions. Free-air gravity and magnetic anomaly values in region no: 1 represent inverse (opposite) correlation. By the way, the crustal thinning is expected wherein the free-air gravity anomaly increases and magnetization decreases. In the region no: 2, while free-air gravity values decrease, the magnetic anomaly values increase. This can also be assessed by crustal thickening or by an intrusion which increases magnetization. The similar situation seen in region no: 1 is also observed in region no: 3. Therefore, it can be said that the crust is thin in the regions no: 1 and no: 3. But, the proportion of crustal thinning in the region no: 1 is greater than in no: 3. This case can be related with the high difference between the amplitude of the magnetic values of these regions. In a crustal structure affected with the same mass loading, if magnetic anomaly values are quite highly differentiated, a different mechanism most likely deformation within the crust can be expected. Figure 4b shows that the values of profile B - B' and this profile is divided into 3 regions. The values of profile B - B' (Figure 4b) are similar to the profile A - A' values (Figure 4a). In the regions no: 1 and no: 3, the free-air gravity anomaly values increase while the magnetic anomaly values decrease similar to profile A - A'. However, while free-air gravity values in region no: 2 decrease (respect to the general profile), magnetic anomaly values decrease. Therefore, it can be said that there is an important factor in the crust which reduces magnetization in this region. In Figure 4c, the profile C - C' values are seen and the profile is divided into 2 regions. In the region no: 1, high positive magnetic anomaly values are remarkable. In this area, it is possible to mention that the presence of an intrusion with high magnetization in the crust. Additionally, unlike other profiles (A and B, Figures 4a, 4b), the magnetic anomaly values decrease in the region no: 2 and free-air gravity and magnetic anomaly values change inversely. This case can be related with the crustal thinning in this area. The profile D - D' values are seen in Figure 4d and the profile is divided into 2 regions. In profile D - D' (Figure 4d), the magnetic anomaly values are high positive in the region no: 1. The magnetic anomaly values decrease

rapidly between the regions no: 1 and no: 2. Besides, the relationship between free-air gravity anomaly and decreasing magnetic anomaly in the region no: 2 (Figure 4d) is similar to profile C - C' (Figure 4c). In the region no:2 (Figure 4d), the amplitude of magnetic anomaly values of D - D' is seen more stable respect to the profiles A, B and C (Figure 4a, b, c). In Figure 4e, the profile E - E' values are drawn and the profile is divided into 4 regions. In the profile E - E' (Figure 4e), high positive magnetic anomaly amplitudes are seen in the region no: 1 as similar as in D profile (Figure 4d). In the region no:2 (Figure 4e), it is seen that while free-air gravity values are increasing and magnetic anomaly values are decreasing, this case is also observed in A and B profiles (Figures 4a, 4b). Although the free-air gravity values in the region no: 3 decreases slightly, a significant increasing and then decreasing is observed in the magnetic anomaly values. In the region no: 4, while not a clear changing is seen in the free-air gravity and the magnetic anomaly values continue to decrease. This condition can be associated with crustal thinning in this region.

In Figure 5, it is seen that 1st order trend applied Bouguer gravity anomaly values change between -30 mGal and 15 mGal. Figure 7 presents the relation between Bouguer gravity (Figure 5) and topography (Figure 6) anomalies for 5 profiles. According to isostasy theorem, if there is an inverse relation between gravity and topography data, there is a local isostatic balancing in the region (Watts, 2001; Pamukçu and Yurdakul, 2008; Çırmık et al., 2017a). In profile A - A' (Figure 7a), the relation between gravity and topography values are approximately inverse throughout the profile, therefore it can be said that there is local balancing. In profile B - B' (Figure 7b), the relation between two data set is inverse from the initial of the profile (~26.4° longitude) to 26.6° longitude and between the longitudes from 26.7° to ~26.78° so it can be said that there is a local isostatic balance in the mentioned locations. On the other hand, it can be said that there is a crustal problem (high pressure, the existence of a liquid, etc.) in the region at 26.62° longitude and its surroundings since both the Bouguer gravity and topography values decrease together. In profile C - C' (Figure 7c), the relation between two data set is inverse between the longitudes from 26.5° to ~26.54° and from 26.66° to

26.69°. Therefore, it can be said that these regions have local isostatic balancing. At similar locations (at 26.62° longitudes and its surroundings) (Figure 7c) with profile B - B′ (Figure 7b), the direct relation between gravity and topographic values are seen, thus, the crustal problem is expected in this location. In the profiles D - D′ (Figure 7d) and E - E′ (Figure 7e), the relation between two data set is inverse generally throughout the profiles. But, this case (decreasing of the Bouguer gravity and topography values together) which shown in the regions at longitude 26.62° and its surroundings is not clear in the profiles D - D′ (Figure 7d) and E - E′ (Figure 7e) as seen in the profiles B - B′ and C - C′ (Figures 7b, c). As a result, some parts of the study area have an uncompensated mechanism.

In the other step, the deviatoric stress values (Figure 8) were obtained by using the mean density values and the Bouguer gravity anomaly values for investigating the horizontal stress distribution created by gravitational loadings. The deviatoric stress values change from -0.2 MPa to 0.1 MPa in the study region (Figure 8). Additionally, the Coulomb stress changes and its components normal and shear stress changes were calculated for investigating the changes of stress and were drawn together (Figures 9, 10 and 11) with deviatoric stress values for evaluating the changes more clearly. In Figure 9, the Coulomb stress and deviatoric stress values are negative at GFZ and its surroundings (Figure 1). In the eastern part of GFZ (at Urla and its surroundings, Figure 1) and SW of the study region, the deviatoric stress values are high positive but these regions represent average (approximately zero) Coulomb stress values (Figure 9). Controversially, NW of the study region while representing positive (higher than average) Coulomb stress values, show average (approximately zero) deviatoric stress values. SE of the study region represents similar features in both coulomb and deviatoric stress maps. In the normal stress and deviatoric stress (Figure 10) maps, it is seen that only centre of GFZ represents similar features (negative values) in both maps. The southern and northern parts of GFZ represent average normal stress values and no coherency with deviatoric stress. Besides, NE of the study region has negative normal stress values while its deviatoric stress values are high positive. Also, the normal and deviatoric stress values of SE, SW and NW of the study area are coherent with

each other (Figure 10). In Figure 11, it is seen that the shear stress values of southern and central parts of GFZ and also SE of the study area are consistent with the deviatoric stress values. Besides, the shear stress values of Urla and its surroundings are more coherent with deviatoric stress values respect to Coulomb (Figure 9) and normal stresses (Figure 10). As a general result, the area which is located between the longitude 26.6° and latitudes between 38.3° - 38.4° (GFZ and its surroundings) has negative Coulomb, normal, shear and deviatoric stress values. In Figure 8, the area between the longitudes 26.6° - 26.7° represent the highest negative deviatoric stress values. In Figure 11, it is seen that this area also has negative shear stress values (which were obtained from horizontal movements based on GNSS) and deviatoric stress values (obtained from gravity values) therefore it can be said that GFZ represents completely the sense of strike - slip fault in this area.

The decreasing of the gravity and topographic value amplitudes in the B - B′ (Figure 7b) and C - C′ (Figure 7c) profiles is fit with the area between the longitudes 26.6° - 26.7° which represents the highest negative deviatoric stress values seen in Figure 8. According to the isostatic compensated mechanism, while the topographic values decrease / increase, gravity value is expected to increase / decrease. In the parts of B - B′ (Figure 7b) and C - C′ (Figure 7c) profiles where come across with the highest negative deviatoric stress valued region (Figure 8), the isostatic compensated mechanism is not seen. Therefore, it can be thought that a physical factor may affects the density in these parts.

Additionally, the mean density estimations of the subsurface structure in the study area were calculated with Parasnis method by using Bouguer anomaly values and topography values at 5 profiles (Figure 5) (Table 1). The density, which was found as 2.59 gr / cm^3 in the north of the study region, decreased to 2.06, 1.8 and 1.49 gr / cm^3 towards to the south. Based on the detailed geological map of the study region, it can be said that this extreme density reduction may be caused by sedimentary, volcanic tuff and pyroclastic rock units (Sözbilir et al., 2009; Uzel et al., 2012). Baba et al. (2019) pointed out the existence of possible geothermal resources in the study area. The locations of the possible geothermal resources may be related

to the regions including low density and negative magnetization and uncompensated region which were found in this study.

The area which is located between the longitudes ~26.6° - 26.63° and the latitude 38.3° (Figure 8), where is closer to region no: 2 of the B - B′ profile (Figure 4b) both the gravity and magnetic values decrease. Therefore, it can be said that there is an effective factor which reduces the magnetic features in these locations and its surroundings. Additionally, this region represents negative amplitude deviatoric, coulomb shear and normal stress values (Figures 8 - 11) and high negative Bouguer anomaly values (Figure 5). In the magnetic map (Figure 3) and correspondence analysis of the profiles (Figure 4), it is seen that the magnetic anomalies reduce rapidly and represent negative amplitudes in the south of the study region. This finding is consistent with the distributions (reducing from north to south) of the mean density values of the crust (Table 1). The highest reducing (approximately -500 nT) in the magnetic anomaly (Figure 4b) coincides with the location at longitude ~26.62° (Figure 8). In this region, which has negatively high stress values, the existence of hot

crustal materials rising to shallower depths and high deformation at lower crust can be thought.

The earthquakes occurred between the years 1970 and 2020 with M>4 which were obtained from United States Geological Survey (USGS) were drawn in Figure 12. If these earthquake distributions are investigated with the deviatoric stress (Figure 12), it is seen that there is no any earthquake at the region which has high negative deviatoric stress values.

The region which has no seismicity (Figure 12) has also high negative Coulomb (Figure 9), normal (Figure 10) and shear (Figure 11) stress anomalies. Additionally, the Bouguer gravity anomalies (Figure 5) represent high negative values in this region. Therefore, it can be said that the crustal structure of the region may be ductile. Because, if the density of the crust is lower than the expected values, the form of crust is ductile, so seismicity is not expected. In addition, this idea is supported by the existence of the geothermal sources (Baba et al., 2019) and the findings related with the crust thinning (Figure 4) and the non-isostatic balance conditions (Figure 7) in the study area.
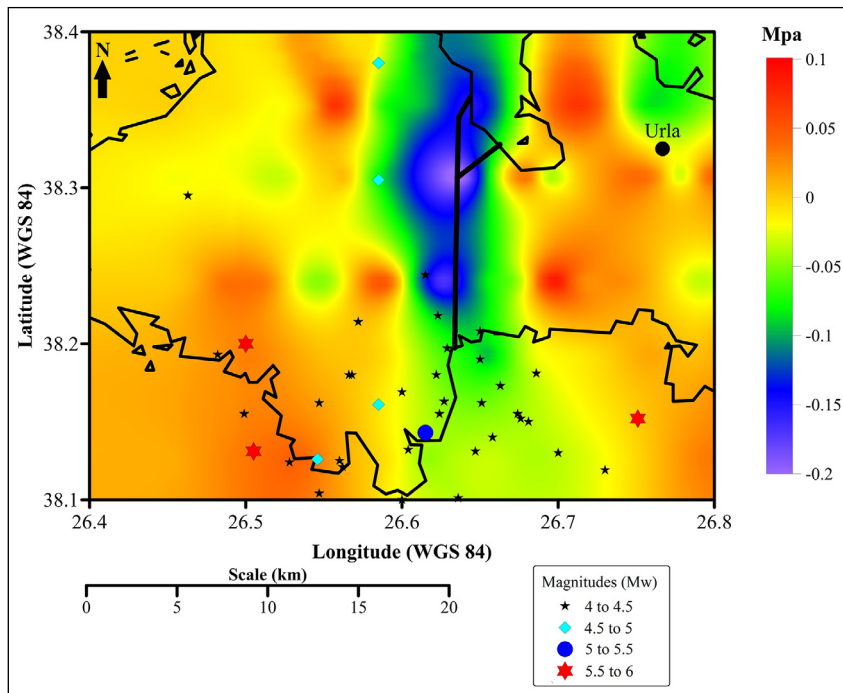
Figure 12- The deviatoric stress values with the earthquakes occurred between the years 1970 - 2020 (M > 4). The earthquake data was obtained from United States Geological Survey (USGS, 2021; https://earthquake.usgs.gov/earthquakes/search/).

Acknowledgements

References

Aadnoy, B., Looyeh, R. 2019. Petroleum Rock Mechanics: Drilling Operations and Well Design. Gulf Professional Publishing. 460.

Akıncı, A., Eyidoğan, H., Göktürkler, G., Akyol, N., Ankaya, O. 2000. İzmir ili çevresinin depremselliği ve deprem tehlikesinin incelenmesi. Batı Anadolu'nun Depremselliği Sempozyumu (BADSEM 2000) İzmir, Bildiri Kitabı, 231-238 (in Turkish).

Aktuğ, B., Kılıçoğlu, A. 2006. Recent crustal deformation of İzmir, Western Anatolia and surrounding regions as deduced from repeated GPS measurements and strain field. Journal of Geodynamics 41, 471-484.

Ambraseys, N. N. 1988. Engineering seismology. Earthquake Engineering Structural Dynamical 17, 1–105.

Arslan, S., Akın, U., Alaca, A. 2010. Gravite verileri ile Türkiye'nin kabuk yapısının incelenmesi. Bulletin of the Mineral Research and Exploration 140, 57-73.

Baba, A, Şaroğlu, F., Akkuş, I., Özel, N., Yeşilnacar, M. İ., Nalbantçılar, M. T., Demir, M. M., Gökçen, G., Arslan, Ş., Dursun, N., Uzelli, T., Yazdani, H. 2019. Geological and hydrogeochemical properties of geothermal systems in the southeastern region of Turkey. Geothermics 78, 255-271.

Barka, A. A., Kadinsky Cade, K. 1988. Strike-slip fault geometry in Turkey and its influence on earthquake activity. Tectonics 7, 663-684.

Bozkurt, E. 2001. Neotectonics of Turkey- a synthesis. Geodinamica Acta 14, 3-30.

Çetiner, M. 2012. İzmir ve çevresindeki mikrogravite verilerinin değerlendirilmesi. MSc Thesis, Dokuz Eylül University, The Graduate School of Nature and Applied Sciences, 78, İzmir.

Çırmık, A., Özdağ, O. C., Doğru, F., Pamuk, E., Gönenç, T., Akgün, M., Arslan, A. T. 2016. The soil behaviours of the GNSS station. Earth Sciences 5(5), 70-81.

Çırmık, A., Pamukçu, O. 2017. Clarifying the interplate main tectonic elements of Western Anatolia, Turkey by using GNSS velocities and Bouguer gravity anomalies. Journal of Asian Earth Science 148, 294-304.

Çırmık, A., Doğru, F., Gönenç, T., Pamukçu, O. 2017a. The stress / strain analysis of kinematic structure at Gülbahçe Fault and Uzunkuyu Intrusive (İzmir, Turkey). Pure and Applied Geophysics 174(3), 1425-1440.

Çırmık, A., Pamukçu, O., Gönenç, T., Kahveci, M., Şalk, M., Herring, T. 2017b. Examination of the kinematic structures in İzmir (Western Anatolia) with repeated GPS observations (2009, 2010 and 2011). Journal of African Earth Sciences 126, 1-12.

De Ritis, R., Ventura, G., Chiappini, M., Carluccio, R., Von Frese, R. 2010. Regional magnetic and gravity anomaly correlations of the Southern Tyrrhenian Sea. Physics of the Earth and Planetary Interiors 181(1-2), 27-41.

Dewey, J. F., Şengör, A. M. C. 1979. Aegean and surrounding regions: complex multi plate and continuum tectonics in a convergent zone. Geological Society of America Bulletin Part 1 90, 84-92.

Doğru, F., Pamukçu, O. 2019. Analysis of gravity disturbance for boundary structures in the Aegean Sea and Western Anatolia. Geofizika 36(1), 53-76.

Doğru, F., Pamukçu, O., Gönenç, T., Yıldız, H. 2018. Lithospheric structure of western Anatolia and the Aegean Sea using GOCE-based gravity field models. Bollettino di Geofisica Teorica ed Applicata 59(2), 135-160.

Doğru, F., Pamukçu, O., Özsöz, I. 2017. Application of tilt angle method to the Bouguer gravity data of Western Anatolia. Bulletin of the Mineral Research and Exploration 155(155), 213-222.

Emre, Ö., Özalp, S., Doğan, A., Özaksoy, V., Yıldırım, C., Göktaş, F. 2005. İzmir yakın çevresinin diri fayları ve deprem potansiyelleri. Maden Tetkik Arama Genel Müdürlüğü, Rapor No: 10754, Ankara (unpublished).

Erbek, E., Dolmaz, M. N. 2014. Geophysical researches (gravity and magnetic) of the Eratosthenes Seamount in the eastern Mediterranean Sea. Acta Geophysica 62(4), 762-784.

Heiskanen, W. A., Moritz, H. 1967. Physical geodesy. Bulletin Geodesique 86, 491–492.

Hinze, W. J., Von Frese, R. R. B., Saad, A. H. 2013. Gravity and Magnetic Exploration Principles, Practices and Applications. Cambridge University Press, 502.

Göktaş, F. 2016. Ildır Körfezi güneyindeki bölgenin Neojen stratigrafisi Çeşme Yarımadası, Batı Anadolu. Türkiye Jeoloji Bülteni 59(3), 299–321 (in Turkish).

Ketin, İ. 1948. Uber die tektonisch - mechanischen Folgerungenaus den grossen Anotolischen Erdbeben des letzten Dezenniums. Geologische Rundschau 36, 77-83.

Malaliçi, B. C. 2019. Gülbahçe fayı ve çevresinin jeodinamik yapısının irdelenmesi. MSc Thesis, Dokuz Eylül University, The Graduate School of Nature and Applied Sciences, 77, İzmir.

McKenzie, D. 1972. Active tectonics of the Mediterranean region. Geophysical Journal of the Royal Astronomical Society 30, 109-185.

Mount, V. S., Suppe, J. 1987. State of stress near the San Andreas fault: implications for wrench tectonics. Geology 15(12), 1143-1146.

Ocakoğlu, N., Demirbağ, E., Kuşçu, İ. 2005. Neotectonic structures in İzmir Gulf and surrounding regions (western Turkey): evidences of strike-slip faulting with compression in the Aegean extensional regime. Marine Geology 219(2-3), 155-171.

Pamuk, E. 2019. Investigating edge detection, Curie point depth, and heat flow using EMAG2 magnetic and EGM08 gravity data in the northern part of Eastern Anatolia, Turkey. Turkish Journal of Earth Sciences 28(6), 805-821.

Pamukçu, O. 2017. Stress analysing with gravity data. 3. International Conference on Engineering and Natural Science, 3 - 7 May 2017, Budapest, 600-602.

Pamukçu, O. A., Akçığ, Z. 2011. Isostasy of the Eastern Anatolia (Turkey) and discontinuities of its crust. Pure and Applied Geophysics 168(5), 901-917.

Pamukçu, O., Yurdakul, A. 2008. Isostatic compensation in Western Anatolia with estimate of the effective elastic thickness. Turkish Journal of Earth Sciences 17, 545-557.

Pamukçu, O., Akçığ, Z., Demirbaş, Ş., Zor, E. 2007. Investigation of crustal thickness in eastern Anatolia using gravity, magnetic and topographic data. Pure Applied Geophysics 164, 2345-2358.

Pamukçu, O., Gönenç, T., Çırmık, A., Pamukçu, Ç., Ertürk, N. 2019. The geothermal potential of Büyük Menderes Graben obtained by combined 2.5 - D normalized full gradient results. Pure and Applied Geophysics 176(11), 5003-5026.

Pamukçu, O., Gönenç, T., Çırmık, A., Sındırgı, P., Kaftan, I., Akdemir, Ö. 2015. Investigation of vertical mass changes in the south of İzmir (Turkey) by monitoring microgravity and GPS/GNSS methods. Journal of Earth System Science 124(1), 137-148.

Pamukçu, O., Gönenç, T., Yurdakul, A., Kahveci, M. 2013. Sismik riski yüksek olan İzmir - Karaburun'un güneyinde yapılmış mikrogravite ve GPS çalışmaları. Jeofizik 18, 59-66.

Pamukçu, O., Gönenç, T., Yurdakul, A., Özyalın, Ş., Sözbilir, H. 2012. Application of boundary analysis and modelling methods on Bouguer gravity data of the Gediz Graben and surrounding area in Western Anatolia and its tectonic implications. Journal of the Balkan Geophysical Society 15, 19-30.

Parasnis, D. S. 1952. A study of rock densities in English Midlands. Geophysical Journal International 6, 252–271.

Saleh, S., Jahr, T., Jentzsch, G., Saleh, A., Abou Ashour, N. M. 2006. Crustal evaluation of the northern Red Sea rift and Gulf of Suez, Egypt from geophysical data: 3-dimensional modeling. Journal of African Earth Sciences 45(3), 257–278.

Sözbilir, H., Softa, M., Eski, S., Tepe, Ç., Akgün, M., Pamukçu, O., Çırmık, A., Utku, M., Özdağ, C. Ö., Özden, G., Özçelik, Ö., Evlek, D. A., Çakır, R., Baba, A., Uzelli, T., Tatar, O. 2020. 30 October 2020 Sisam (Samos) Earthquake (Mw: 6.9) Evaluation Report, Dokuz Eylül University Earthquake Research and Application Center (in Turkish).

Sözbilir, H., Sümer, Ö., Uzel, B., Ersoy, Y., Erkül, F., İnci, U., Helvacı, C. Özkaymak, Ç. 2009. 17 - 20 Ekim 2005 - Sığacık Körfezi (İzmir) depremlerinin sismik jeomorfolojisi ve bölgedeki gerilme alanları ile ilişkisi, Batı Anadolu. Türkiye Jeoloji Bülteni, 52 (2), 217–238 (in Turkish).

Şengör, A. M. C., Yılmaz, Y. 1981. Tethyan evolution of Turkey: a plate tectonic approach. Tectonophysics 75, 181-241.

Şengör, A. M. C., Görür, N., Şaroğlu, F. 1985. Strike - slip faulting and related basin formation in zones of tectonic escape: Turkey as a case study. Special Publications of the Society of Economic Palaeontologists and Mineralogists 37, 227–264.

Taymaz, T., Jackson, J., McKenzie, D. P. 1991. Active tectonics of the North and Central Aegean Sea. Geophysical Journal International 106, 433–490.

Turcotte, D. L., Schubert, G. 2002. Geodynamics. Cambridge University Press, 456.

USGS (United States Geological Survey earthquake catalog). https://earthquake.usgs.gov/earthquakes/search/. 1 June 2021.

Uzel, B., Sözbilir, H. 2008. A first record of strike - slip basin in western Anatolia and its tectonic implication: The Cumaovası basin as an example. Turkish Journal of Earth Sciences 17, 559–591.

Uzel, B., Sözbilir, H., Özkaymak, Ç. 2012. Neotectonic evolution of an actively growing superimposed basin in western Anatolia: the inner bay of Izmir, Turkey. Turkish Journal of Earth Sciences 21(4), 439-471.

Von Frese, R. R. B., Hinze, W. J., Braile, L. W. 1982. Regional North American gravity and magnetic anomaly correlations. Geophysical Journal International 69, 145-761.

Von Frese, R. R., Jones, M. B., Kim, J. W., Kim, J. H. 1997*a*. Analysis of anomaly correlations. Geophysics 62(1), 342-351.

Von Frese, R. R., Jones, M. B., Kim, J. W., Li, W. S. 1997*b*. Spectral correlation of magnetic and gravity anomalies of Ohio. Geophysics 62(1), 365-380.

Watts, A. B. 2001. Isostasy and Flexure of the Lithosphere. Cambridge University Press, 458.

Xu, C., Wang, H. H., Luo, Z. C., Ning, J. S., Liu, H. L. 2015. Multilayer stress from gravity and its tectonic implications in urban active fault zone: a case study in Shenzhen, South China. Journal of Applied Geophysics 114, 174-182.